ChemPlusChem
Full Papers
doi.org/10.1002/cplu.202000395
Chem
Europ
European C
Societies P

Special Collection

ThDione: A Powerful Electron-Withdrawing Moiety for Push–Pull Molecules

Eva Novotná,[a] Iwan V. Kityk,[b] Oldřich Pytela,[a] Filip Bureš,*[a] Miroslav Ludwig,[a] Milan Klikar,*[a] Katarzyna Ozga,[b] and Jaroslaw Jedryka[b]

Dedicated to Iwan V. Kityk

A series of new push–pull chromophores based on a combined cyclopenta[*c*]thiophene-4,6-dione (ThDione) acceptor, *N*,*N*-dimethylaniline, *N*-piperidinylthiophene or ferrocene donors, and ethylene or buta-1,3-dienylene π-linkers has been designed and synthesized. Utilizing one or two ThDione acceptors afforded linear or branched push–pull molecules. Experimental and theoretical study of their fundamental properties revealed thermal robustness up to 260 °C, a electrochemical/optical HOMO–LUMO gap that is tunable within the range of 1.47–2.19/1.99–2.39 eV, and thorough elucidation of structure–property relationships. Compared to currently available portfolio of heterocyclic electron-withdrawing units, ThDione proved to be a powerful and versatile acceptor unit. It imparts significant intramolecular charge transfer and polarizes the π-system, which results in enhanced (non)linear optical response.

Introduction

Organic π-systems with D-π-A/push-pull arrangement belong to prominent organic chromophores with extraordinary optoelectronic properties and wide applications.[1–4] During the last decades, a plethora of donor-π-acceptor molecules has been synthesized and utilized across material chemistry fields such as dyes, colorants, active layers of organic devices, emitters, nonlinear optical (NLO) media, switches etc.[5–27] A push-pull molecule can easily be designed by a combination of available electron releasing/withdrawing substituents interconnected by various π-systems. To this date, a large number of donor/acceptor groups has been developed and well-examined.[28] Beside elementary D/A substituents with mesomeric effect such as alkoxy, diakylamino, cyano or nitro, more complex and advanced D/A units based on heterocyclic systems or multi-heteroatom sequences have also been designed.[29] 1,3-Dicarbonyl compounds represent very popular group of electron withdrawing moieties, mostly due to their instant availability and active methylene moiety, which allows their easy incorporation into the chromophore backbone via Knoevenagel condensation. Indan-1,3-dione is a typical example of powerful yet simple acceptor with 1,3-dicarbonyl arrangement and fused benzene ring, which allows further delocalization. We have recently demonstrated its first structural modification on the fused benzene ring affording novel T-shaped push-pull chromophores.[30–32] Malonic acid and its derivatives, namely cyanoacetic acid, malononitrile, dialkyl malonate, Meldrum's or (thio)barbituric acid, are another class of popular acceptors with related 1,3-dicarbonyl arrangement.[33] Fundamental optoelectronic properties of push-pull chromophores are considerably affected by the intramolecular charge-transfer (ICT) between the particular donor and acceptor mediated via a π-system. Hence, polarizability of the used π-system is also an important aspect which has to be taken into account. Whereas six-membered (hetero)aromatic compounds are considered as electron deficient, five-membered rings are generally electron rich. However, we have demonstrated that proper decoration of five-membered heteroaromatic compounds such as imidazole, thiazole or thiophene with electron withdrawing substituents may reverse their electronic behavior and dicyanoimidazole, dicyanothiazole, dicyanothiophene or dinitrothiophene may be used as electron withdrawing moieties of push-pull chromophores.[34–39] Thiophene is inherent, highly polarizable, and electron rich heteroaromatics referred to as auxiliary donor.[38,40] Its electronic properties are often further modified by sulfur oxidation,[41] or fusing with another (hetero)aromatic compound, e.g. thienothiophene,[42] isothianaphtene[43] or benzothiadiazoles.[44–46]

Considering the aforementioned structural aspects, we have recently designed and prepared cyclopenta[*c*]thiophene-4,6-dione (ThDione, Figure 1).[42,47,48] It combines polarizable electron rich thiophene and 1,3-dicarbonyl arrangement similar to that in indan-1,3-dione or malonic acid derivatives, while presence of CH_2 moiety allows its facile introduction via Knoevenagel condensation. According to the very recent comparison of the most popular electron withdrawing moieties, ThDione proved

---

[a] E. Novotná, Prof. O. Pytela, Prof. F. Bureš, Prof. M. Ludwig, Dr. M. Klikar
Institute of Organic Chemistry and Technology
University of Pardubice
Faculty of Chemical Technology
Studentská 573, Pardubice, 53210 (Czech Republic)
E-mail: filip.bures@upce.cz
milan.klikar@upce.cz
[b] Prof. I. V. Kityk, Prof. K. Ozga, Dr. J. Jedryka
Chair of Control Engineering
Electrical Engineering and Optoelectronics,
Czestochowa University of Technology
Al. Armii Krajowej 17, Czestochowa, 42-200 (Poland)

Supporting information for this article is available on the WWW under https://doi.org/10.1002/cplu.202000395

Special Collection *This article is part of a Special Collection on "Chemistry in the Czech Republic".*

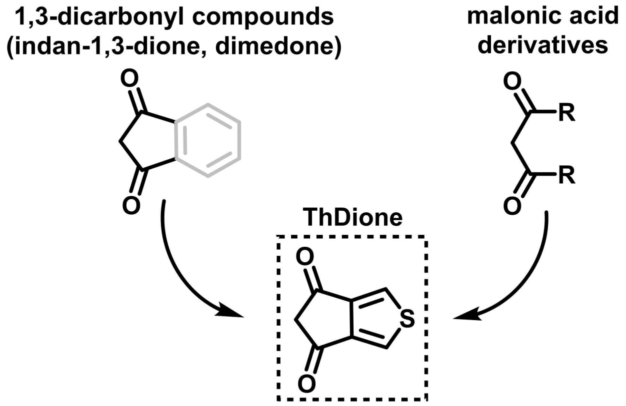

Figure 1. Relation between popular 1,3-dicarbonyl electron acceptors.

to be powerful acceptor comparable to tricyanovinyl or thiobarbituric acid.[42]

However, since today no systematic study of its connection to various electron donors has been carried out. Figure 2 shows structure of novel D-π-A and A-π-D-π-A systems with ThDione acceptor and three representative electron donors that include widely used *N*,*N*-dimethylaniline (DMA), very powerful 2-(piperidin-1-yl)thiophene (PIT),[33] and organometallic ferrocene (Fc). Olefinic π-system has been selected to allow efficient ICT between both D and A parts. We present herein a thorough structure-property relationship study based on evaluation of thermal, (opto)electronic, and DFT data.

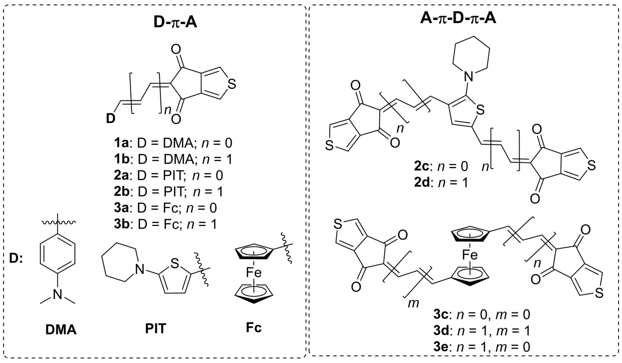

Figure 2. General structures of target molecules **1**–**3**.

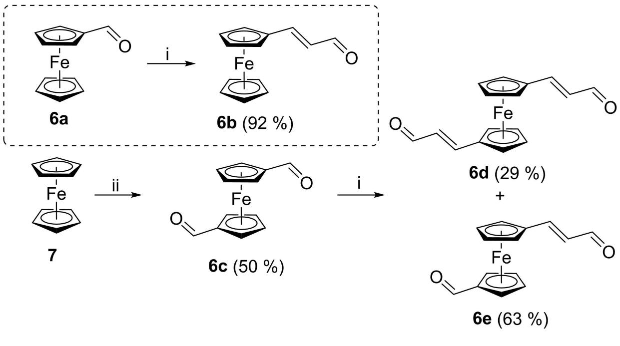

Scheme 1. Synthesis of ferrocene aldehydes **6 b**–**e**: i) 1. Tributyl (1,3-dioxolan-2-ylmethyl)phosphonium bromide, NaH, THF, 25 °C, 12 h; 2. HCl, THF, 25 °C, 1 h (Method A). ii) 1. *n*-BuLi, hexane, TMEDA, 25 °C; 2. DMF, 0 °C, 2 h; 3. HCl.

Results and Discussion

Synthesis

The synthesis of all target chromophores is based on simple Knoevenagel condensation between an aldehyde and ThDione. DMA aldehydes **4 a**–**b** and ferrocenecarboxaldehyde **6 a** are commercial available. The preparations of PIT aldehydes **5 a**–**d** and ThDione were described earlier.[33,47] As depicted in Scheme 1, aldehyde **6 c** was prepared by twofold direct formylation of ferrocene **7**.[49] Well-established protocol employing tributyl (1,3-dioxolan-2-ylmethyl)phosphonium bromide has been utilized for Wittig olefination (Method A).[50] Starting from **6 a**, extended aldehyde **6 b** was obtained in high 92 % yield. Similar twofold olefination of **6 c** yielded a 1 : 2 mixture of aldehydes **6 d** and **6 e** (overall 92 % yield), which was successfully separated by a column chromatography on alumina.

With all desired aldehydes in hand, the final Knoevenagel condensation employing ThDione was carried out (Scheme 2, Method B). Piperidine was used as suitable catalyst which assured sufficient reactivity of ThDione with all types of aldehydes. Despite similar in principle, the separation and purification of the Knoevenagel products were the most challenging. Target molecules, especially chromophores **2 c**–**d** and **3 c**–**e** with elongated and planarized π-linkers, are sparingly soluble in common solvents used for chromatography. Moreover, some chromophores underwent partial hydrolysis during chromatography affording starting aldehyde and ThDione. Intense degradation occurred for Fc chromophore **3 b** which could be isolated in diminished 3 % yield. All chromophores were further crystallized and, therefore, the isolated yields are generally low, which mostly reflects their difficult purification.

Thermal analysis

Thermal behavior of all target molecules **1**–**3** (except **3 b**) was examined by different scanning calorimetry (DSC). Figure 3

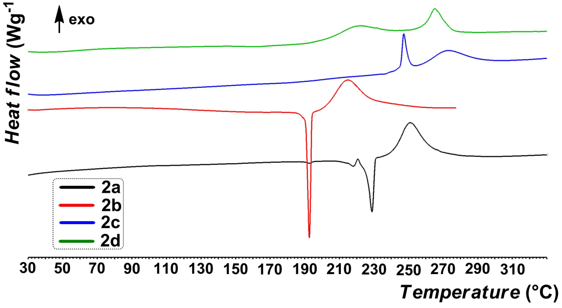

Figure 3. Representative DSC curves of compounds **2 a**–**d** (PIT chromophores) determined with a scanning rate of 3 °C/min under N_2 atmosphere.

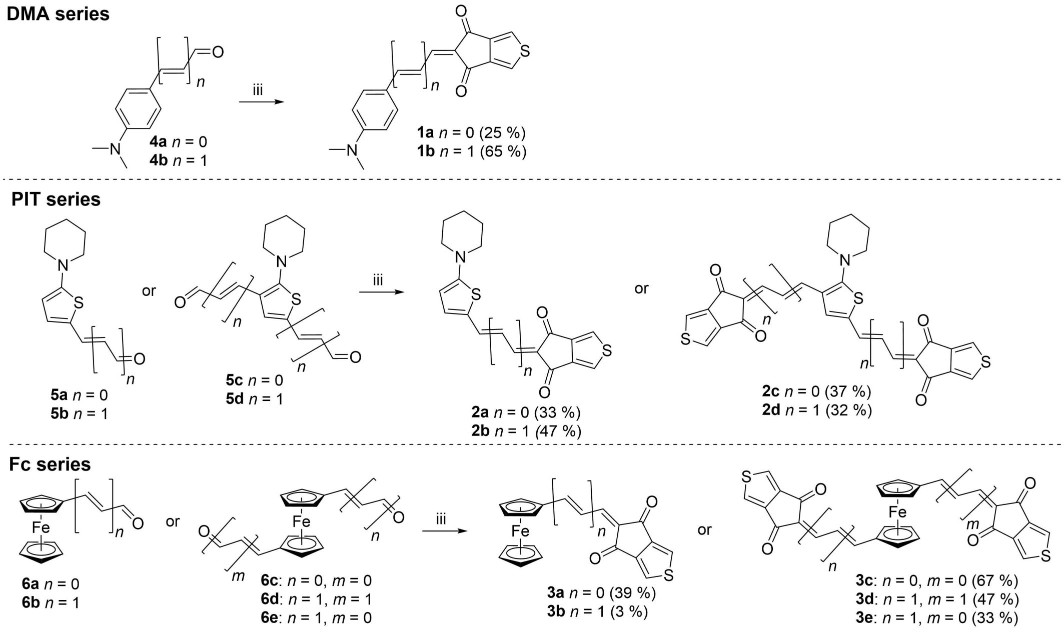

Scheme 2. Synthesis of target chromophores **1**–**3** (Method B): iii) ThDione, piperidine, CH_2Cl_2 or CH_3CN, 25 °C, 16 h.

shows thermograms of representative compounds **2 a**–**d** while Table 1 lists all measured melting points (T_m) and temperatures of thermal decompositions (T_d). All DCS records are provided in the Supporting Information. The measured melting points and temperature of decomposition range from 172–250 and 195–260 °C, respectively. Linear **1 a**–**b**, **2 a**–**b**, and **3 a** melted sharply and their liquid phase proved unstable with immediate decomposition during following heating process (T_d exceeded T_m by about 5–25 °C). On the contrary, branched **2 c**–**d** decomposed directly without previous melting. Their degradation generally took place in two consecutive steps (e.g. Figure 3). Decomposition of branched ferrocene derivatives **3 c**–**e** is also represented by two exothermic steps; the first one is broad and less pronounced, the second one is sharp and vigorous.

Based on the performed DSC analysis the following outcomes can be deduced:

- π-Linker elongation reduces thermal robustness in DMA and PIT series (see Figure 3, **2 a**/**c** vs. **2 b**/**d**, $\Delta T_d = 40$–50 °C). In general, thermal robustness may be improved by introducing rigid (hetero)aromatic or organometallic moieties, simple connectors such as olefinic or acetylenic bridge bring rather

Table 1. Summary of thermal, electrochemical, and optical properties of chromophores **1**–**3**.

Comp.	T_m [°C][a]	T_d [°C][b]	$E_{p(ox1)}$ [V][d]	$E_{p(red1)}$ [V][d]	$\triangle E$ [V][d]	E_{HOMO} [eV][e]	E_{LUMO} [eV][e]	$\lambda_{max}{}^{A}$ [nm/eV][f]	$\varepsilon_{max}{}^{A} \times 10^3 [M^{-1} \cdot cm^{-1}]$[f]
1a	237	260	0.98	−1.21	2.19	−5.37	−3.18	494/2.51	60
1b	250	255	0.76	−0.98	1.74	−5.15	−3.41	551/2.25	47
2a	225	240	0.73	−1.27	2.00	−5.12	−3.12	529/2.34	96
2b	190	200	0.48	−0.99	1.47	−4.87	−3.40	622/1.99	72
2c	/	245	0.94	−0.88	1.82	−5.33	−3.51	577/2.15	47
2d	/	195	0.72	−0.82	1.54	−5.11	−3.57	591/2.10	46
3a	172	195	0.66	−1.20	1.86	−5.05	−3.19	367/3.38 583/2.13[g]	11 3[g]
3b	[c]	[c]	0.63	−0.96	1.59	−5.02	−3.43	416/2.98 602/2.06[g]	18 7[g]
3c	/	195	0.83	−1.03	1.86	−5.22	−3.36	333/3.72 518/2.39[g]	42 7[g]
3d	/	200	0.72	−0.93	1.65	−5.11	−3.46	378/3.28 570/2.18[g]	75 14[g]
3e	/	210	0.79	−0.92	1.71	−5.18	−3.47	349/3.55 533/2.33 [g]	46 10[g]

[a] T_m = melting point (the point of intersection of a baseline and a tangent of thermal effect = onset). [b] T_d = thermal decomposition (pyrolysis in N_2 atmosphere). [c] Not measured. [d] $E_{p(ox1)}$ and $E_{p(red1)}$ are peak potentials of the first oxidation and reduction (irreversible processes), respectively, as measured by CV at scan rate 100 mV s^{-1}; all potentials are given *vs.* SSCE; $\Delta E = E_{p(ox1)} - E_{p(red1)}$. [e] $-E_{HOMO/LUMO} = E_{p(ox1/red1)} + 4.35$ (in DMF vs. SCE)[51] + 0.036 [difference between SCE (0.241 vs. SHE) and SSCE (0.205 vs. SHE)].[52] [f] Measured in CH_2Cl_2 at concentration 10^{-5} M. [g] Absorption maxima corresponding to HE and LE bands.

thermal instability. However, introducing olefinic linker has less negative effect on thermal robustness as compared to other acetylenic chromophores.[34,41–42]

- Compared to **1** and **2**, the ferrocene compounds **3** possess slightly reduced thermal stability as judged by their lower T_d values. Nevertheless, presence of the ferrocene moiety suppresses negative effect of the olefinic linker and **3 a**–**e** showed almost identical T_d values (195–210 °C).
- T_d values are comparable between analogical pairs of compounds with D-π-A and A-π-D-π-A structural arrangement (**2 a**/**2 b**/**3 a** vs. **2 c**/**2 d**/**3 c**, $\Delta T_d \approx 5$ °C). Hence, the branching of chromophore structure does not influence its thermal robustness.
- Thermal stability is mainly dictated by the type of donor with the order: Fc < PIT < DMA. The highest thermal stability was recorded for DMA chromophore **1 a** ($T_d = 260$ °C).

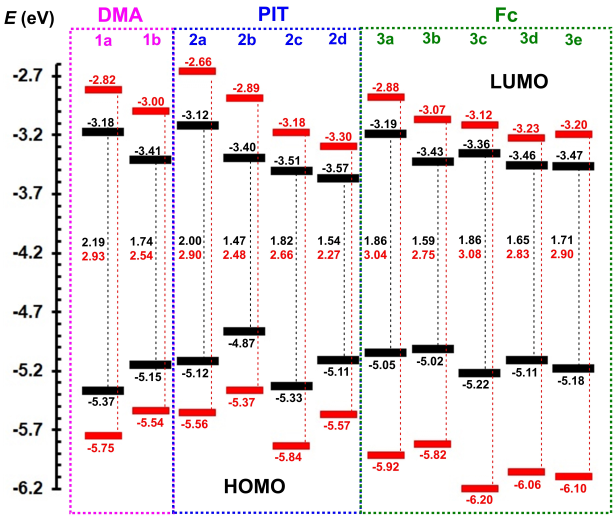

Figure 4. Energy level diagram of electrochemical (black) and DFT calculated (red) values for chromophores **1**–**3**.

Electrochemistry

Electrochemical investigation of chromophores **1**–**3** were carried out in DMF containing 0.1 M Bu_4NBF_4 in a three electrode cell by cyclic voltammetry (CV). The acquired data are summarized in Table 1, all CV diagrams are shown in Fig. S7 and S8 (see the Supporting Information).

The first oxidations and reductions are irreversible processes followed by additional oxidations and reductions. Quasi-reversible reductions were detected only for linear chromophores **1 a**, **2 a**, and **3 a**. The first reductions were determined as one-electron and the first oxidations as one or multiple-electron processes (especially for DMA and Fc series). It is well-know that the ferrocene first oxidation involves iron(II) redox center as fully reversible process.[36] However, Fc derivatives **3 a**–**e** underwent irreversible first oxidation, which points to a significant D–A interaction of ferrocene donor with ThDione acceptor. Both potentials of the first oxidation/reduction are certainly a function of particular chromophore structure. The recorded peak potentials $E_{p(ox1/red1)}$ were recalculated to $E_{HOMO/LUMO}$ values and these are visualized in the energy level diagram in Figure 4.

Based on the electrochemical measurements, the following relationships can be deduced:

- LUMO: Chromophores with the same π-linker showed almost constant LUMO level (e.g. **1 b**/**2 b**/**3 b**, $E_{LUMO} = -3.41/\ -3.40/\ -3.43$ eV). Thus, it is obvious that LUMO must be localized on ThDione electron withdrawing moiety. The LUMO level is mostly affected by elongation and branching of the π-system.
- HOMO: Chromophores within particular series possess different E_{HOMO} values, which indicates the HOMO localization at the DMA, PIT or Fc donor. The HOMO level is further controlled by the π-system length and branching. Embedding ethenylene unit increases the E_{HOMO} by 0.03–0.25 eV, whereas it becomes deepened when going from D-π-A to A-π-D-π-A arrangement (e.g. **2 a** vs. **2 c**, −5.12 vs. −5.33 eV).
- Compared to DMA and PIT molecules, the structural modifications affect the HOMO/LUMO levels in Fc derivatives **3 a**–**e** less significantly (Figure 4). The HOMO-LUMO gap is generally given by the π-system extension, the effect of the branching and the number of ThDione acceptors is diminished.
- The Δ*E* of unsymmetrical Fc derivative **3 e** lies between those measured for **3 c** and **3 d**.
- In **1**–**2**, the HOMO–LUMO gap is clearly controlled by the type of donor, π-linker length, and the number of acceptor units. However elongation of the π-system has the most pronounced effect on reducing Δ*E* (e.g. **1 a** vs. **1 b**, Δ*E* = 2.19 vs.1.74 eV). Linear and branched chromophores exhibited similar Δ*E* values (e.g. **2 b** vs. **2 d**, Δ*E* = 1.47 vs.1.54 eV), which implies that structural branching deepened both the HOMO and LUMO, but their difference remained almost unaltered.
- Chromophore **2 b** with PIT donor and elongated π-system showed the narrowest HOMO–LUMO gap of 1.47 eV.

Linear optical properties

All target chromophores **1**–**3** are intensely colored solids; their color ranges from yellow to dark blue (Figure S9 in the Supporting Information). Due to the strong ICT, no emission has been detected. The absorption spectra were recorded in three solvents with different polarity (toluene, CH_2Cl_2, and DMF). The longest absorption maxima (λ_{max}) and their corresponding molar extinction coefficients (ε_{max}) are summarized in Table 1 and S1. The absorption spectra in CH_2Cl_2 are shown in Figure 5, all spectra are depicted in Figures S10–S12.

All linear D-π-A chromophores **1 a**–**b**, **2 a**–**b**, and **3 a**–**b** exhibited one distinct CT-absorption peak corresponding to a strong D–A interaction. On the contrary, branched A-π-D-π-A chromophores **2 c**–**d** and **3 c**–**e** possess one dominant CT-band with an additional shoulder shifted either hypsochromically (PIT series) or bathochromically (Fc series). This splitting of the absorption bands is due to a coupling between branches and reflects quadrupolar arrangement of target chromophores **2 c**–**d**

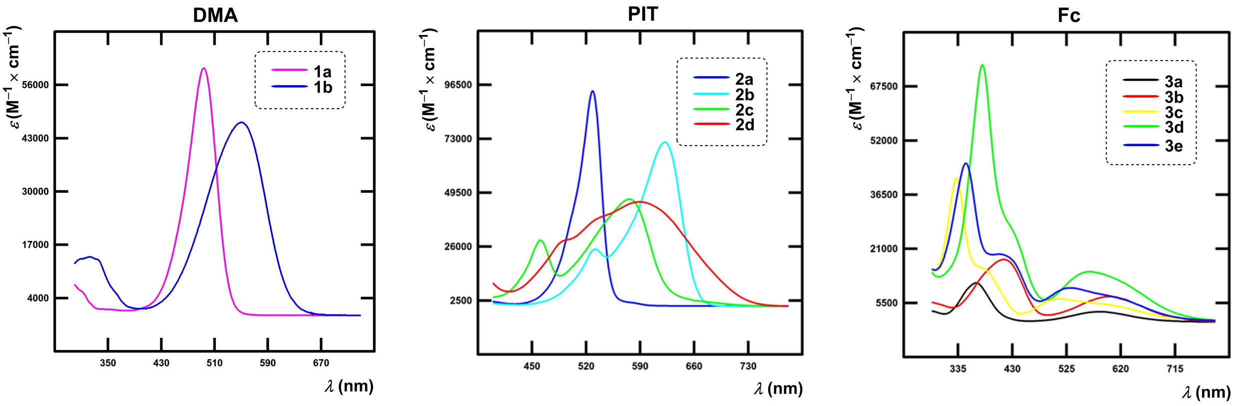

Figure 5. UV-Vis absorption spectra of target chromophores in CH_2Cl_2 (10^{-5} M).

and **3c**–**e**.[53] Moreover, the ferrocene is considered as a donor with dual ICT from the cyclopentadienyl (Cp) and Fe moieties.[36] Whereas the Cp→ThDione interaction is observed as high energy (HE) band, the Fe→ThDione interaction is shifted to low energy (LE) and appears as a weak peak. Both HE and LE peaks are clearly observed in solvents with low polarity, e.g. toluene and CH_2Cl_2. In polar aprotic DMF, both peaks are merged together and appear as a structured bands with one or more shoulders. The absorption maxima of **3a**–**e** in DMF range between 450–520 nm and are localized between the high and low energy bands found in toluene/CH_2Cl_2. A correlation of electrochemical and optical gaps ($1240/\lambda_{max}$) is very tight for chromophores **1a**–**b** and **2a**–**d** with standard mesomeric DMA and PIT donors. The ferrocene derivatives **3a**–**e** were clearly identified as outliers (Figure S13 in the Supporting Information). This observation corroborates aforementioned electrochemical behavior of **3a**–**e** and points to a specific solute-solvent interaction in DMF.

Considering the linear optical properties, we can deduce the following relationships:

- Elongation of the π-system by ethenylene spacer induces a significant bathochromic shift of 20–90 nm.
- When going from linear D-π-A to quadrupolar A-π-D-π-A systems, the molar extinction coefficient either decrease (e.g. PIT derivatives **2b** vs. **2d**, $\Delta\varepsilon_{max} = -24 \times 10^3\ M^{-1}cm^{-1}$) or increase (e.g. Fc derivatives **3c** vs. **3a**, $\Delta\varepsilon_{max} = 37 \times 10^3\ M^{-1}cm^{-1}$).
- CT-band positioning of linear and branched analogues obey the Frankel exciton model.
- The longest-wavelength absorption peak in **1** and **2** with amino-based donors undergo significant hypsochromic shift upon protonation (see the Figure S14). The original band may be regenerated upon neutralization with trimethylamine, which confirm its CT nature.
- Asymmetric Fc derivative **3e** possesses the CT-band localized between the absorption maxima of symmetric analogues **3c** and **3d**.
- A comparison of the absorption maxima for analogous chromophores with different donors (e.g. **1b**, **2b**, **3b**) demonstrates their donating ability (PIT > Fc > DMA). The most red-shifted absorption maxima was measured for linear chromophore **2b** ($\lambda_{max} = 622$ nm), which feature PIT donor and extended π-system. On the contrary, the most hypsochromically shifted CT-band was observed for DMA chromophore **1a** ($\lambda_{max} = 494$ nm).
- When comparing the absorption maxima measured in different solvents (Table S1), a slight bathochromic shift occurs when going from nonpolar toluene to polar DMF. The positive solvatochromism indicates more polar excited state.

Nonlinear optical properties

The fundamental nonlinear optical responses of chromophores **1**–**3** were preliminarily investigated by laser stimulated second- and third-harmonic generation (SHG and THG) of the light. The experimental set-up and details are provide in the Supporting Information. The SHG and THG measurements were carried out with powder samples and a 1064 nm Nd:YAG laser source beam employing reflected light geometry.

Figure 6 shows the dependency between the SHG and the fundamental energy density. The data is referenced to $Ba(BO_2)_2\delta$: 5%Nd (BBOδ) crystal. The maximal energy density was about 100 Jm^{-2}; the higher densities caused sample degradation (especially for **2b**). At first sight, there are remarkable differences between the particular NLOphores.

Most of the samples showed relatively weak SHG response slightly above the noise level. For Fc-chromophores **3**, the SHG signal increases to a certain level and then rapidly decreases to the noise level, which is associated with their photo-degradation. However, chromophores **1b** and **2c** provided a clear green SHG signal at 532 nm with the intensity about 15% lower as compared to the reference crystal. Both chromophores possess strong DMA or PIT donors and extended or branched π-system, respectively.

THG responses vs. fundamental laser energy for the particular chromophores are given in Figure 7. To prevent sample degradation, the maximal energy was reduced to

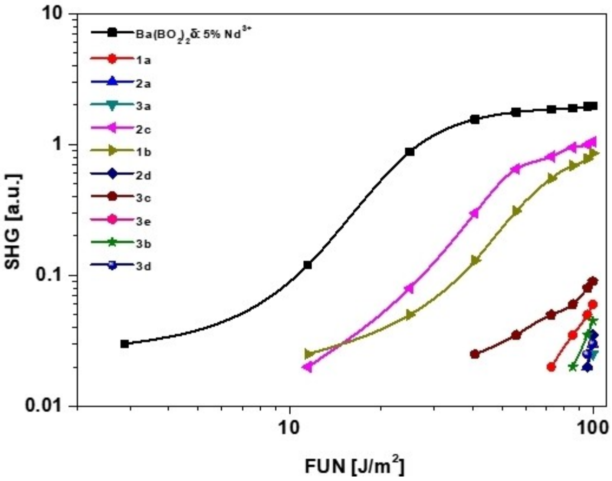

Figure 6. SHG vs. fundamental energy density for **1**–**3**.

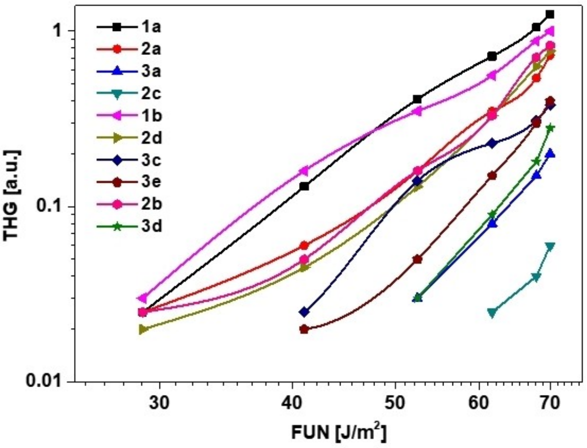

Figure 7. THG vs. fundamental energy density for **1**–**3**.

70 Jm^{-2}. In general, DMA and PIT chromophores **1** and **2** showed the best performance. In contrast to SHG measurements, chromophore **2c** possesses weak third-order NLO activity. Despite its non-centrosymmetric quadrupolar molecular arrangement (see below), it may adopt a centrosymmetric supramolecular layout with a diminished response. All remaining chromophores in the series **2** showed a clear THG signal. However, simple DMA- and ThDione-terminated chromophores **1a** and **1b** proved to be the most efficient third-order NLOphores, especially at lower energy densities. The THG response of ferrocene chromophores **3** was about 50% lower as compared to **1** and **2**.

Theoretical calculations

Spatial and electronic properties of target chromophores were investigated using Gaussian® 16 W software[54] package at the DFT level. Initial geometries of molecules **1**–**3** were optimized by DFT B3LYP/6-311+G(2d,f,p) method. Energies of the frontier molecular orbitals, their differences ΔE and ground state dipole moments μ were calculated at DFT B3LYP/6-311++G(3d,f,2p) level in DMF. The first hyperpolarizabilities β were computed at DFT B3LYP/6-311++G(3d,f,2p) level in vacuum at 1064 nm. Theoretical electronic absorption spectra were calculated at TD-DFT (nstates=8) B3LYP/6-311++G(3d,f,2p) level in vacuum and corresponding λ_{max} values were deduced. All calculated data are summarized in Table 2.

The calculated HOMO and LUMO energies range from −6.20 to −5.37 and −3.30 to −2.66 eV and are clearly dependent on the structural arrangement of the particular chromophore as can be seen from the energy level diagram in Figure 4. As deduced from the experimental and calculated data, both obtained LUMO levels correlate tightly (Figure S16). Compared to experimental values, the calculated HOMO levels for Fc derivatives **3** are negatively shifted. The difference is probably due to a specific interactions of **3** measured in DMF (see above). However, the theoretical HOMO levels obey the same trends as those measured by cyclic voltammetry. A correlation of both quantities as well as the HOMO-LUMO gaps splits into two sections (**1**+**2** vs. **3**) with high correlation coefficients (Figures S17-18). These tight correlations indicate that theoretical calculations are capable to describe similar structure-property relationships as seen by the electrochemical measurements. Namely, elongation of the π-linker via double bond(s) reduces the energy gap in the most pronounced way. The calculated data also shows that the HOMO-LUMO gap is affected by the chromophore branching. The lowest gaps were calculated for PIT chromophores **2**.

The HOMO/LUMO localizations were calculated at DFT B3LYP/6-311+G(2d,f,p) level using DFT-optimized geometries

Table 2. DFT-calculated properties of chromophores **1**–**3**.

Comp.	E_{HOMO} [eV][a]	E_{LUMO} [eV][a]	ΔE[a] [eV]	μ [a] [D]	λ_{max}[c] [nm/eV]	$\beta\times10^{-30}$ [esu][b]	GoS[e]
1a	−5.75	−2.82	2.93	8.9	418/2.97	206	C_s
1b	−5.54	−3.00	2.54	12.5	462/2.68	761	C_s
2a	−5.56	−2.66	2.90	12.4	431/2.88	146	non
2b	−5.37	−2.89	2.48	17.3	475/2.61	691	non
2c	−5.84	−3.18	2.66	7.7	501/2.48	445	non
2d	−5.57	−3.30	2.27	9.7	544/2.28	3540	non
3a	−5.92	−2.88	3.04	2.3	380/3.26 642/1.93[d]	18	non
3b	−5.82	−3.07	2.75	4.8	400/3.10 630/1.97[d]	404	non
3c	−6.20	−3.12	3.08	2.2	453/2.74 732/1.69[d]	4	C_2
3d	−6.06	−3.23	2.83	1.4	447/2.77 678/1.83[d]	36	C_2
3e	−6.10	−3.20	2.90	3.0	461/2.69 705/1.76[d]	346	non

[a] Calculated at the DFT B3LYP/6-311++G(3d,f,2p) level in DMF. [b] Calculated at the DFT B3LYP/6-311++G(3d,f,2p) level in vacuum at 1064 nm (−2ω;ω,ω). [c] Calculated at the TD-SCF (nstates=8) B3LYP/6-311++G(3d,f,2p) level in vacuum. [d] Absorption maxima corresponding to HE and LE bands. [e] Group of symmetry.

and visualized in OPchem.[55] The frontier molecular orbitals in representative chromophores **1 b**, **2 b**, and **3 b** are shown in Figure 8; for complete listing see the Supporting Information. In linear chromophores with mesomeric donors (DMA and PIT), the HOMO-1 is spread over the ThDione C1-C3 atoms and the adjacent π-linker, similarly to the LUMO+1. This reflects combination of electron-rich thiophene with electron-withdrawing cyclopentandione moieties of ThDione. The HOMO/LUMO are generally localized over the central π-system involving both donors and acceptors. Branched molecules **2 c** and **2 d** possess the HOMO-1/LUMO+1 spread over one branch, while HOMO/LUMO is localized centrally. In Fc derivatives **3 a**–**b**, the HOMO-1 is centralized on the Fe atom. The LUMO+1 is spread over either the ferrocene or ThDione moieties. The branched chromophores **3 c**–**e** possess the frontier molecular orbitals centrally localized involving ferrocene and adjacent π-system of both branches.

The linear DMA and PIT chromophores **1 a**–**b** and **2 a**–**b** showed higher dipolar character resulting in the larger ground state dipole moments ($\mu = 9$–17 D). Quadrupolar molecules **2 c**–**d** and ferrocene derivatives possess diminished dipole moments of 1–10 D. The calculated second-order polarizabilities β obey quite similar trends. Whereas Fc derivatives **3** possess modest NLO coefficients, DMA and PIT derivatives **1**–**2** showed higher NLO activity. Overestimated β value for PIT derivative **2 d** should be considered as outlier. The π-linker elongation (e.g. **2 a**/**2 b**→146/691 $\times 10^{-30}$ esu) and branching (e.g. **2 a**/**2 c**→146/445 $\times 10^{-30}$ esu) generally enhances the calculated NLO response. On the contrary, molecular symmetrization via structural branching significantly suppresses the β polarizabilities; for instance see the non-symmetric and C_2-symmetric **3 b** and **3 d** with β equal to 404 and 36×10^{-30} esu, respectively. The largest NLO coefficients β were calculated for DMA and PIT chromophores **1 b** (761×10^{-30} esu) and **2 b** (691×10^{-30} esu) with enlarged π-systems. This is in a very good agreement to the aforementioned experimental values.

Figure 9 shows a representative electronic absorption spectra of chromophore **3 a** overlapped with the experimental one; for complete listing see the Supporting Information. The calculated λ_{max}^{DFT} values are listed in Table 2. As can be deduced from Figures 9 and S22–24, TD-DFT spectra are either blue- or red-shifted for DMA **1** and PIT series **2** ($\Delta\lambda_{max} \approx 50$–150 nm/0.2–0.6 eV) and Fc **3** (when considering both HE and LE bands). However, both theoretical and experimental UV-Vis spectra possess the same bands and shoulders. The calculated longest-wavelength absorption maxima are affected by the same structural features as discussed for the experimental ones measured in dichloromethane. According to the analysis of the particular oscillators, the CT-band of chromophores **1**–**2** consists of the HOMO→LUMO transition. The high energy shoulders of branched PITs **2 c**–**d** correspond to the HOMO→LUMO+1 transition. As expected, the LE bands of **3** are originated from the HOMO→LUMO transition with weaker oscillator strength, while the HE bands are generated by the subsequent transitions (from HOMO-2 to LUMO+2) and possess larger oscillator strength.

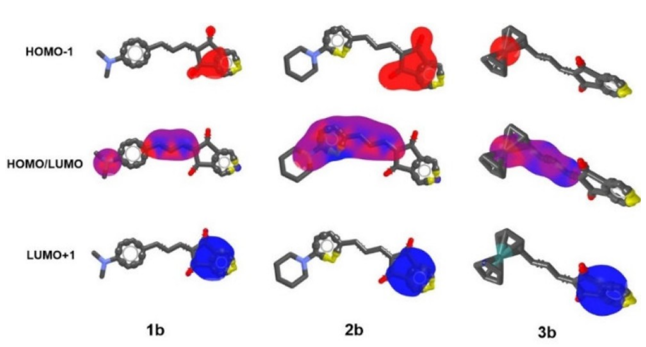

Figure 8. The HOMO (red) an LUMO (blue) localizations in representative chromophores **1 b**, **2 b**, and **3 b**.

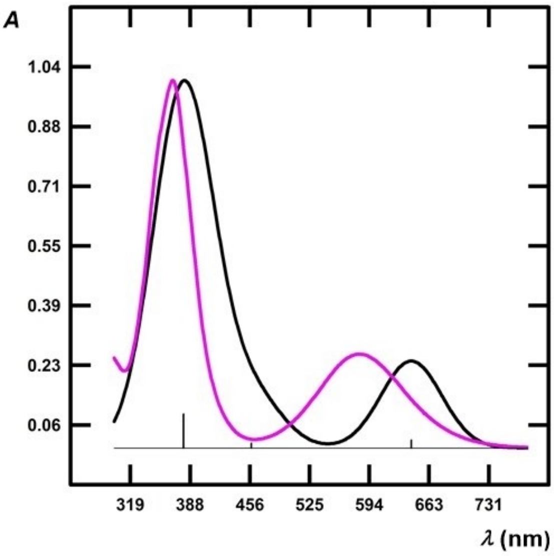

Figure 9. TD-DFT calculated (black) and experimentally obtained (violet) UV-Vis spectra of chromophore **3 a** in CH_2Cl_2. Both spectra were overlapped and normalized to have maximal absorbance (A) of 1.

Conclusion

Inspired by very successful and widely used indan-1,3-dione, ThDione combines highly polarizable thiophene ring fused with cyclopentan-1,3-dione bearing active methylene group. It represents an electron-withdrawing moiety, which features facile preparation and allows easy introduction via Knoevenagel condensation. Its systematic employment as electron acceptor was investigated on a series of D-π-A and A-π-D-π-A molecules with three widely used electron donors. All prepared chromophores showed thermal robustness sufficiently high to be considered as materials suitable for organic electronics. We have demonstrated extensive property tuning in terms of varying their fundamental parameters such as HOMO-LUMO gap and optical properties. Both parameters are tunable within a wide range by introducing one or two ThDione acceptors, chromophore branching, replacing the appended electron donor, and varying the interconnecting π-system. These structural features have influenced also their nonlinear optical properties that were preliminarily screened by SHG and THG. All experimental data are corroborated by DFT calculations. We believe that this contribution will serve as useful guide for organic and material chemists looking for new and powerful heterocyclic acceptor moiety.

Experimental Section

General methods

All target chromophores **1**–**3** are new compounds. The preparation and characterization of ferrocene aldehydes **6 b**–**e** are given in the Supporting Information. All commercial chemicals, reagents and solvents were purchased from suppliers such as Sigma Aldrich, TCI, Acros, Penta at reagent grade and were used as obtained. The dry THF was always freshly distilled from Na/K alloy and benzophenone under an inert atmosphere of argon. The preparations of ferrocene aldehydes **6 b**–**e** were carried out in flame-dried flasks under argon. Column chromatography was carried out with silica gel or alumina and commercially available solvents. Thin-layer chromatography (TLC) was conducted on aluminum sheets coated with SiO_2 or Al_2O_3 (60 F_{254}), obtained from Merck, with visualization by a UV lamp (254 or 360 nm). Melting points of **6 b**–**e** were determined by using Büchi B-540 instrument in open capillaries. Thermal properties of all target chromophores were measured by differential scanning calorimetry with a Mettler-Toledo STARe System DSC 2/700 equipped with FRS 6 ceramic sensor and cooling system HUBER TC100-MT RC 23. The measurements were carried out in open aluminous crucibles under N_2 inert atmosphere. DSC curves were determined with a scanning rate of 3 °C/min within the range 25–400 °C. Melting point and temperature of decomposition were determined as intersection of baseline and tangent of peak (onset point). ^1H and ^{13}C NMR spectra were recorded at 400 and 100 MHz, respectively, with a Bruker AVANCE 400/500 instrument or 500 and 125 MHz, respectively, with Bruker Ascend™ 500 at 25 °C. Chemical shifts are reported in ppm relative to the signal of Me_4Si. The residual solvent signal in the ^1H and ^{13}C NMR spectra was used as an internal reference ($CDCl_3$ 7.25 and 77.23 ppm). Apparent resonance multiplicities are described as s (singlet), d (doublet), dd (doublet of doublet), t (triplet) and m (multiplet); the coupling constants of multiplets (^3J or ^4J) are given in Hz. High resolution MALDI MS spectra were measured on a MALDI mass spectrometer LTQ Orbitrap XL (Thermo Fisher Scientific, Bremen, Germany) equipped with nitrogen UV laser (337 nm, 60 Hz). The LTQ Orbitrap instrument was operated in positive-ion mode over a normal mass range (*m/z* 50–2000) with resolution 100 000 at *m/z* = 400. The survey crystal positioning system (survey CPS) was set for the random choice of shot position by automatic crystal recognition. 2,5-Dihydroxybenzoic acid (DHB) was used as a matrix. Mass spectra were averaged over the whole MS record for all measured samples. The absorption spectra were measured on a Hewlett-Packard 8453 spectrophotometer in toluene, CH_2Cl_2, and DMF at c $\approx 1\times10^{-5}$ M. The IR spectra were measured on a FT-IR Nicolet iS50 spectrometer with a diamond ATR adapter. The electrochemical behavior of target chromophores were investigated by cyclic voltammetry in DMF containing 0.1 M Bu_4NPF_6 in a three electrode cell by cyclic voltammetry (CV). The working electrode was glassy carbon disk (1 mm in diameter). Leak-less Ag/AgCl electrode (SSCE) containing filling electrolyte (3.4 M KCl) and titanium rod with a thick coating of platinum were used as the reference and auxiliary electrodes. All peak potentials are given *vs.* SSCE. Voltammetric measurements were performed by using an integrated potentiostat system ER466 (eDAQ Europe, Warszawa, Poland) operated with EChem Electrochemistry software. The set-up used for NLO measurements is given in the Supporting Information.

General Method B (Knoevenagel condensation)

The Knoevenagel condensation was carried out according to modified procedure.[56] ThDione (100 mg, 0.66 mmol) and corresponding aldehyde (0.44/0.26 mmol for mono/twofold condensation) were dissolved in CH_2Cl_2 (30 mL; for **1 a**, **2 b**–**c**, and **3 a**–**e**) or CH_3CN (30 mL; for **1 b**, **2 a**, and **2 d**) and piperidine (5 drops) was added. The reaction mixture was stirred at 25 °C for 18 hours. The solvent was evaporated in *vacuo* and the crude product was purified by column chromatography and crystallized from CH_2Cl_2/hexane mixture (2:1).

Chromophore (1 a)

The title compound was prepared from DMA aldehyde **4 a** (66 mg) following the general method B. Chromophore **1 a** was obtained as a pink solid (31 mg, 25 %). $R_f = 0.8$ (SiO_2; CH_2Cl_2/EtOAc 3:1). ^1H-NMR (500 MHz, $CDCl_3$, 25 °C): $\delta = 3.14$ (s, 6H, $N(CH_3)_2$), 6.72 (d, 2H, $J = 9.0$ Hz, Ph), 7.74 (s, 1H, CH), 7.84 (d, 1H, $J = 2.2$ Hz, ThDione), 7.85 (d, 1H, $J = 2.2$ Hz, ThDione), 8.49 ppm (d, 2H, $J = 9.0$ Hz, Ph). ^{13}C-NMR (125 MHz, $CDCl_3$, 25 °C): $\delta = 40.3$, 111.6, 122.1, 124.1, 124.2, 131.1, 138.5, 146.0, 147.6, 149.3, 154.3, 183.6, 185.0 ppm. FT-IR (HATR): $\nu =$ 3068, 2918, 1702, 1648, 1524, 1468, 1357, 1232, 1142, 1060, 1004, 818 cm^{-1}. HR-FT-MALDI-MS (DHB) *m/z* calcd. for $C_{16}H_{14}NO_2S^+$ ($[M+H]^+$): 284.07398; found 284.07336 ($\Delta = 2.18$ ppm).

Chromophore (1 b)

The title compound was prepared from DMA aldehyde **4 b** (77 mg) following the general method B. Chromophore **1 b** was obtained as a dark purple solid (89 mg, 65 %). $R_f = 0.8$ (SiO_2; CH_2Cl_2/EtOAc 3:1). ^1H-NMR (500 MHz, $CDCl_3$, 25 °C): $\delta = 3.08$ (s, 6H, $N(CH_3)_2$), 6.68 (d, 2H, $J = 9.0$ Hz, Ph), 7.28 (d, 1H, $J = 15.0$ Hz, CH), 7.58 (d, 2H, $J = 9.0$ Hz, Ph), 7.61 (d, 1H, $J = 12.0$ Hz, CH), 7.84 (d, 1H, $J = 2.2$ Hz, ThDione), 7.85 (d, 1H, $J = 2.2$ Hz, ThDione),, 8.24 ppm (dd, 1H, $J_1 = 15.0$ Hz, $J_2 = 12.0$ Hz Ph). ^{13}C-NMR (125 MHz, $CDCl_3$, 25 °C): $\delta = 40.4$, 111.6, 119.4, 123.9, 124.2, 124.4, 131.8, 132.4, 146.6, 147.6, 148.5, 152.8, 154.4, 184.1, 184.6 ppm. FT-IR (HATR): $\nu = 2905$, 1645, 1521, 1463, 1360, 1308, 1273, 1221, 1113, 990, 758 cm^{-1}. HR-FT-MALDI-MS (DHB) *m/z* calcd. for $C_{18}H_{16}NO_2S^+$ ($[M+H]^+$): 310.08963; found 310.08874 ($\Delta = 2.87$ ppm).

Chromophore (2 a)

The title compound was prepared from PIT aldehyde **5 a** (86 mg) following the general method B. Chromophore **2 a** was obtained as a gold-brown solid (48 mg, 33 %). $R_f = 0.6$ (SiO_2; CH_2Cl_2/EtOAc 3:1). ^1H-NMR (400 MHz, $CDCl_3$, 25 °C): $\delta = 1.72$–1.75 (m, 6H, $3\times CH_2$), 3.56–3.58 (m, 4H, $2\times CH_2$), 6.27 (d, 1H, $J = 4.8$ Hz, Th), 7.54 (d, 1H, $J = 2$ Hz, Th), 7.63 (d, 1H, $J = 2.4$ Hz, ThDione), 7.68 (d, 1H, $J = 2.4$ Hz, ThDione), 7.71 ppm (s, 1H, CH).^{13}C-NMR (125 MHz, $CDCl_3$, 25 °C): $\delta =$ 23.8, 25.5, 51.6, 108.0, 122.1, 122.6, 123.1, 136.9, 138.0, 146.5, 147.1, 149.8, 173.4, 184.4, 185.0 ppm. FT-IR (HATR): $\nu = 2934$, 2855, 1683, 1626, 1462, 1361, 1240, 1153, 1075, 1004, 748 cm^{-1}. HR-FT-MALDI-MS (DHB) *m/z* calcd. for $C_{17}H_{16}NO_2S_2^+$ ($[M+H]^+$): 330.06170; found 330.06121 ($\Delta = 1.48$ ppm).

Chromophore (2 b)

The title compound was prepared from PIT aldehyde **5 b** (98 mg) following the general method B. Chromophore **2 b** was obtained as a dark green-blue solid (70 mg, 45%). $R_f = 0.7$ (SiO_2; EtOAc). ^{1}H-NMR (500 MHz, $CDCl_3$, 25 °C): $\delta = 1.68$–1.73 (m, 6H, 3×CH_2), 3.40–3.42 (m, 4H, 2×CH_2), 6,08 (d, 1H, $J = 4.5$ Hz, Th), 7.20 (d, 1H, $J = 4.5$ Hz, Th), 7.33 (d, 1H, $J = 14.0$ Hz, CH), 7.50 (d, 1H, $J = 12.5$ Hz, CH), 7.72–7.78 ppm (m, 3H, CH + ThDione).^{13}C-NMR (125 MHz, $CDCl_3$, 25 °C): $\delta = 23.8$, 25.3, 51.6, 106.3, 117.3, 122.9, 123.3, 126.3, 129,7, 139.6, 146.6, 146.7, 147.6, 147.7, 167.4, 184.5, 185.1 ppm. FT-IR (HATR): $\nu =$ 3088, 2922, 2849, 2111, 1680, 1632, 1565, 1520, 1409, 1337, 1206, 1059, 979, 744 cm^{-1}. HR-FT-MALDI-MS (DHB) *m/z* calcd. for $C_{19}H_{18}NO_2S_2^+$ ($[M+H]^+$): 356.07735; found 356.07714 ($\Delta =$ 0.59 ppm).

Chromophore (2 c)

The title compound was prepared from PIT aldehyde **5 c** (59 mg) following the general method B. Chromophore **2 c** was obtained as a dark purple solid (47 mg, 37%). $R_f = 0.6$ (SiO_2; CH_2Cl_2/EtOAc 3 : 1). ^{1}H-NMR (500 MHz, $CDCl_3$, 25 °C): $\delta = 1.78$–1.89 (m, 6H, 3×CH_2), 3.69–3.71 (m, 4H, 2×CH_2), 7.65 (s, 1H, Th), 7.82 (d, 1H, $J = 2.0$ Hz, ThDione), 7.86 (d, 1H, $J = 2.2$ Hz, ThDione), 7.87 (s, 1H, CH), 7.92 (d, 1H, $J = 2.0$ Hz, ThDione), 7.95 (d, 1H, $J = 2.2$ Hz, ThDione), 8.92 ppm (s, 1H, CH).^{13}C-NMR (125 MHz, $CDCl_3$, 25 °C): $\delta = 23.8$, 25.9, 56.8, 118.7, 123.3, 124.3, 124.5, 125.1, 125.3, 129.0, 131.5, 136.4, 139.2, 145.8, 146.4, 146.9, 147.4, 150.2, 178.7, 182.9, 183.6, 183.8, 183.9 ppm. FT-IR (HATR): $\nu = 3100$, 2919, 1707, 1658, 1550, 1453, 1369, 1276, 1212, 1152, 1063, 945, 755 cm^{-1}. HR-FT-MALDI-MS (DHB) *m/z* calcd. for $C_{25}H_{18}NO_4S_3^+$ ($[M+H]^+$): 492.03925; found 492.03951 ($\Delta = 0.53$ ppm).

Chromophore (2 d)

The title compound was prepared from PIT aldehyde **5 d** (72 mg) following the general method B. **2 d** is sparingly soluble in common organic solvents which limits its purification via column chromatography or crystallization. Chromophore **2 d** was obtained as a dark purple solid (45 mg, 32%). $R_f = 0.6$ (SiO_2; CH_2Cl_2/EtOAc 3 : 1). Although **2 d** provides dark colored solutions, it is sparingly soluble in common solvents for NMR analysis. ^{1}H NMR spectra showed a mixture of **2 d** and residual highly soluble impurities roll up from baseline. Hence, the purity of **2 d** cannot be verified via NMR analysis but only by using TLC. Despite this fact, the structure of **2 d** was confirmed by HR-MS analysis. FT-IR (HATR): $\nu = 3078$, 2928, 1705, 1659, 1555, 1451, 1399, 1141, 1060, 987, 827, 760 cm^{-1}. HR-FT-MALDI-MS (DHB) *m/z* calcd. for $C_{29}H_{22}NO_4S_3^+$ ($[M+H]^+$): 544.07055; found 544.07286 ($\Delta = 4.25$ ppm).

Chromophore (3 a)

The title compound was prepared from Fc aldehyde **6 a** (94 mg) following the general method B. Chromophore **3 a** was obtained as a purple solid (60 mg, 39%). $R_f = 0.9$ (SiO_2; CH_2Cl_2/EtOAc 3 : 1). ^{1}H-NMR (500 MHz, $CDCl_3$, 25 °C): $\delta = 4.22$ (s, 5H, Cp), 4.85–4.86 (m, 2H, Cp), 5.37–5.38 (m, 2H, Cp), 7.84 (s, 1H, CH), 7.89 (d, 1H, $J = 2.0$ Hz, ThDione), 7.91 ppm (d, 1H, $J = 2.0$ Hz, ThDione).^{13}C-NMR (125 MHz, $CDCl_3$, 25 °C): $\delta = 71.1$, 75.7, 75.8, 76.4, 124.6, 124.9, 132.1, 145.9, 147.6, 151.3, 183.0, 183.7 ppm. FT-IR (HATR): $\nu = 3109$, 1715, 1665, 1590, 1526, 1478, 1355, 1207, 1000, 828, 765, 475 cm^{-1}. HR-FT-MALDI-MS (DHB) *m/z* calcd. for $C_{18}H_{12}FeO_2S^+$ ($[M]^+$): 347.99019; found 347.99065 ($\Delta = 1.32$ ppm).

Chromophore (3 b)

The title compound was prepared from Fc aldehyde **6 b** (106 mg) following the general method B. The crude product was firstly crystallized and then purified via column chromatography on alumina (Al_2O_3; CH_2Cl_2/hexane 2 : 1). Chromophore **3 b** was obtained as a dark green solid (5 mg, 3%). $R_f = 0.5$ (Al_2O_3; CH_2Cl_2/hexane 2 : 1). ^{1}H-NMR (500 MHz, $CDCl_3$, 25 °C): $\delta = 4.19$ (s, 5H, Cp), 4.63–4.64 (m, 2H, Cp), 4.68–4.69 (m, 2H, Cp), 7.31 (d, 1H, $J = 15.0$ Hz, CH), 7.51 (d, 1H, $J = 12.0$ Hz, CH), 7.88–7.98 ppm (m, 3H, CH + ThDione).^{13}C-NMR (125 MHz, $CDCl_3$, 25 °C): $\delta = 70.0$, 70.6, 73.1, 80.3, 121.7, 124.6, 124.8, 132.5, 146.5, 147.0, 147.6, 155.9, 184.0, 184.4 ppm. FT-IR (HATR): $\nu =$ 3095, 2921, 1710, 1665, 1561, 1476, 1447, 1325, 1143, 992, 762 cm^{-1}. HR-FT-MALDI-MS (DHB) *m/z* calcd. for $C_{20}H_{14}FeO_2S^+$ ($[M]^+$): 374.00584; found 374.00625 ($\Delta = 1.10$ ppm).

Chromophore (3 c)

The title compound was prepared from Fc aldehyde **6 c** (63 mg) following the general method B. Chromophore **3 c** was obtained as a dark purple solid (89 mg, 67%). $R_f = 0.3$ (SiO_2, CH_2Cl_2/EtOAc 5 : 1). ^{1}H-NMR (500 MHz, $CDCl_3$, 25 °C): $\delta = 4.78$ (s, 4H, Cp), 5.43 (s, 4H, Cp), 7.32 (s, 2H, CH), 7.67 ppm (s, 4H, ThDione). ^{13}C-NMR (125 MHz, $CDCl_3$, 25 °C): $\delta = 76.5$, 78.6, 124.6, 124.7, 126.8, 134.0, 145.5, 146.5, 147.2, 182.1, 182.8 ppm. FT-IR (HATR): $\nu = 3064$, 1715, 1672, 1595, 1569, 1526, 1480, 1359, 1209, 1173, 1006, 832, 767, 485 cm^{-1}. HR-FT-MALDI-MS (DHB) *m/z* calcd. for $C_{26}H_{14}FeO_4S_2^+$ ($[M]^+$): 509.96774; found 509.96881 ($\Delta = 2.10$ ppm).

Chromophore (3 d)

The title compound was prepared from Fc aldehyde **6 d** (77 mg) following the general method B. Chromophore **3 d** was obtained as a dark green-purple solid (69 mg, 47%). $R_f = 0.4$ (SiO_2, CH_2Cl_2/EtOAc 5 : 1). ^{1}H-NMR (400 MHz, $CDCl_3$, 25 °C): $\delta = 4.58$ (s, 4H, Fc), 4.62 (s, 4H, Fc), 6.76 (d, 2H, $J = 15.0$ Hz, CH). 7.30 (d, 2H, $J = 12.0$ Hz, CH), 7.49 (dd, 2H, $J_1 = 15.0$ Hz, $J_2 = 12.0$ Hz, CH), 7.62–7.68 ppm (m, 4H, ThDione). ^{13}C-NMR (125 MHz, $CDCl_3$, 25 °C): $\delta = 71.3$, 74.1, 82.8, 123.6, 124.3, 124.4, 133.0, 146.3, 146.5, 147.3, 149.9, 183.3, 183.5 ppm. FT-IR (HATR): $\nu = 3073$, 1704, 1661, 1559, 1475, 1445, 1325, 1145, 980, 768, 486 cm^{-1}. HR-FT-MALDI-MS (DHB) *m/z* calcd. for $C_{30}H_{18}FeO_4S_2^+$ ($[M]^+$): 561.99904; found 562.00006 ($\Delta =$ 1.81 ppm).

Chromophore (3 e)

The title compound was prepared from Fc aldehyde **6 e** (70 mg) following the general method B. Chromophore **3 e** was obtained as a dark green solid (46 mg, 33%). $R_f = 0.5$ (SiO_2, CH_2Cl_2/EtOAc 5 : 1). ^{1}H-NMR (400 MHz, $CDCl_3$, 25 °C): $\delta = 4.57$–4.58 (m, 2H, Cp), 4.68–4.69 (m, 2H, Cp, 4.77–4.78 (m, 2H, Cp), 5.40 –5.41 (m, 2H, Fc), 6.64 (d, 1H, $J = 15.0$ Hz, CH), 7.13 (d, 1H, $J = 12.5$ Hz, CH), 7.29 (s, 1H, CH), 7.45 (dd, 1H, $J_1 = 15.0$ Hz, $J_2 = 12.5$ Hz, CH), 7.64 (d, 2H, $J = 2.2$ Hz, ThDione), 7.84 ppm (d, 2H, $J = 2.3$ Hz, ThDione). ^{13}C-NMR (125 MHz, $CDCl_3$, 25 °C): $\delta = 71.2$, 74.1, 76.5, 76.9, 78.9, 83.7, 122.6, 124.7, 124.8, 124.9, 125.3, 133.1, 133.5, 145.5, 146.0, 146.5, 146.6, 147.1, 147.3, 149.5, 182.4, 183.1, 183.2, 183.3 ppm. FT-IR (HATR): $\nu = 3087$, 1708, 1671, 1589, 1479, 1451, 1360, 1147, 991, 827, 759, 459 cm^{-1}. HR-FT-MALDI-MS (DHB) *m/z* calcd. for $C_{28}H_{16}FeO_4S_2^+$ ($[M]^+$): 535.98339; found 535.98439 ($\Delta = 1.87$ ppm).

Acknowledgements

This research was supported by the Ministry of Education, Youth and Sports of the Czech Republic (LTAIN19101).

Conflict of Interest

The authors declare no conflict of interest.

Keywords: diones · donor–acceptor systems · electrochemistry · (non)linear optics · thiophenes

[1] *Handbook of Organic Materials for Optical and (Opto)Electronic Devices: Properties and Applications (*Ed.: O. Ostroverkhova), Woodhead Publishing, **2013**.

[2] *Organic Optoelectronic Materials* (Ed.: Y. Li), Springer International Publishing, **2015**.

[3] O. Ostroverkhova, *Chem. Rev.* **2016**, *116*, 13279–13412.

[4] Y. Shirota, *J. Mater. Chem.* **2000**, *10*, 1–25.

[5] M. E. Forrest, S. R. Thompson, *Chem. Rev.* **2007**, *107*, 923–1386.

[6] E. A. Miller, R. D. Chandross, *Chem. Rev.* **2010**, *110*, 1–574.

[7] P. N. He, G. S. Tan, L. S. Zheng, Q. Prasad, *Chem. Rev.* **2008**, *108*, 1245–1330.

[8] Y. R. Shen in *The Principles of Nonlinear Optics*, Wiley-Interscience, **2002**.

[9] R. Boyd *Nonlinear Optics*, Academic Press, **2008**.

[10] H. G. Ziarani, G. H. Moradi, R. Lashgari, N. Kruger in *Metal-Free Synthetic Organic Dyes*, Elsevier, **2018**.

[11] *Modern Colorants: Synthesis and Structure* (Ed.: H. S. Peters, A. T. Freeman), Springer, Netherlands, **1995**.

[12] M. Gsänger, D. Bialas, L. Huang, M. Stolte, F. Würthner, *Adv. Mater.* **2016**, *28*, 3615–3645.

[13] S. Shilpi, D. Viresh, *J. Photonics Energy* **2016**, *6*, 025503.

[14] P. K. Bhatnagar in *Nanomaterials and Their Applications. Advanced Structured Materials* (Ed.: Z. H. Khan), Springer, Singapore, **2018**, pp. 261–287.

[15] N. T. Kalyani, H. Swart, S. J. Dhoble in *Principles and Applications of Organic Light Emitting Diodes (OLEDs)*, Woodhead Publishing, **2017**.

[16] T. T. Bui, F. Goubard, M. Ibrahim-Ouali, D. Gigmes, F. Dumur, *Appl. Sci.* **2018**, *8*, 494.

[17] J. H. Lee, C. H. Chen, P. H. Lee, H. Y. Lin, M. K. Leung, T. L. Chiu, C. F. Lin, *J. Mater. Chem. C* **2019**, *7*, 5874–5888.

[18] *Different Types of Field-Effect Transistors - Theory and Applications* (Ed.: M. Pejović), InTechOpen, **2017**.

[19] H. Sirringhaus, *Adv. Mater.* **2014**, *26*, 1319–1335.

[20] L. Torsi, M. Magliulo, K. Manoli, G. Palazzo, *Chem. Soc. Rev.* **2013**, *42*, 8612–8628.

[21] G. A. Chamberlain, *Sol. Cells* **1983**, *8*, 47–83.

[22] O. A. Abdulrazzaq, V. Saini, S. Bourdo, E. Dervishi, A. S. Biris, *Part. Sci. Technol.* **2013**, *31*, 427–442.

[23] J. Gong, K. Sumathy, Q. Qiao, Z. Zhou, *Renewable Sustainable Energy Rev.* **2017**, *68*, 234–246.

[24] K. Sharma, V. Sharma, S. S. Sharma, *Nanoscale Res. Lett.* **2018**, *13*, 381.

[25] A. Hagfeldt, G. Boschloo, L. Sun, L. Kloo, H. Pettersson, *Chem. Rev.* **2010**, *110*, 6595–6663.

[26] N. Fuentes, A. Martín-Lasanta, L. Álvarez De Cienfuegos, M. Ribagorda, A. Parra, J. M. Cuerva, *Nanoscale* **2011**, *3*, 4003–4014.

[27] S. Gao, X. Yi, J. Shang, G. Liu, R. W. Li, *Chem. Soc. Rev.* **2019**, *48*, 1531–1565.

[28] F. Bureš, *RSC Adv.* **2014**, *4*, 58826–58851.

[29] M. Klikar, P. Solanke, J. Tydlitát, F. Bureš, *Chem. Rec.* **2016**, *16*, 1886–1905.

[30] P. Solanke, A. Růžička, T. Mikysek, O. Pytela, F. Bureš, M. Klikar, *Helv. Chim. Acta* **2018**, *101*, e201800090.

[31] P. Solanke, F. Bureš, O. Pytela, M. Klikar, T. Mikysek, L. Mager, A. Barsella, Z. Růžičková, *Eur. J. Org. Chem.* **2015**, *2015*, 5339–5349.

[32] P. Solanke, O. Pytela, F. Bureš, M. Klikar, *Dyes Pigm.* **2019**, *162*, 755–762.

[33] M. Klikar, V. Jelínková, Z. Růžičková, T. Mikysek, O. Pytela, M. Ludwig, F. Bureš, *Eur. J. Org. Chem.* **2017**, *2017*, 2764–2779 .

[34] Z. Hloušková, J. Tydlitát, M. Kong, O. Pytela, T. Mikysek, M. Klikar, N. Almonasy, M. Dvořák, Z. Jiang, A. Růžička, F. Bureš, *ChemistrySelect* **2018**, *3*, 4262–4270.

[35] D. Cvejn, E. Michail, I. Polyzos, N. Almonasy, O. Pytela, M. Klikar, T. Mikysek, V. Giannetas, M. Fakis, F. Bureš, *J. Mater. Chem. C* **2015**, *3*, 7345–7355.

[36] J. Kulhánek, F. Bureš, W. Kuznik, I. V. Kityk, T. Mikysek, A. Růžička, *Chem. Asian J.* **2013**, *8*, 465–475.

[37] J. Kulhánek, F. Bureš, O. Pytela, T. Mikysek, J. Ludvík, A. Růžička, *Dyes Pigm.* **2010**, *85*, 57–65.

[38] J. Kulhánek, F. Bureš, J. Opršal, W. Kuznik, T. Mikysek, A. Růžička, *Asian J. Org. Chem.* **2013**, *2*, 422–431.

[39] J. Kulhánek, M. Ludwig, F. Bureš, J. Tydlitát, *Chem. Heterocycl. Compd.* **2017**, *53*, 46–53.

[40] *Handbook of Thiophene-Based Materials: Applications in Organic Electronics and Photonics* (Ed.: D. F. Perepichka, I. F.; Perepichka), John Wiley & Sons, Ltd, **2009**.

[41] M. Sperátová, J. Jedyrka, O. Pytela, I. V. Kityk, A. H. Reshak, F. Bureš, M. Klikar, *Tetrahedron* **2019**, *75*, 2–11.

[42] J. Podlesný, O. Pytela, M. Klikar, V. Jelínková, I. V. Kityk, K. Ozga, J. Jedryka, M. Rudysh, F. Bureš, *Org. Biomol. Chem.* **2019**, *17*, 3623–3634.

[43] D. Lorcy, K. D. Robinson, Y. Okuda, J. L. Atwood, M. P. Cava, *J. Chem. Soc. Chem. Commun.* **1993**, 345–347.

[44] N. B. Teran, J. R. Reynolds, *Chem. Mater.* **2017**, *29*, 1290–1301.

[45] T. Nakamura, S. Furukawa, E. Nakamura, *Chem. Asian J.* **2016**, *11*, 2016–2020.

[46] T. Higashino, Y. Kurumisawa, S. Nimura, H. Iiyama, H. Imahori, *Eur. J. Org. Chem.* **2018**, *2018*, 2537–2547.

[47] P. Solanke, S. Achelle, N. Cabon, O. Pytela, A. Barsella, B. Caro, F. Robin-le Guen, J. Podlesný, M. Klikar, F. Bureš, *Dyes Pigm.* **2016**, *134*, 129–138.

[48] M. Klikar, P. Le Poul, A. Ružička, O. Pytela, A. Barsella, K. D. Dorkenoo, F. Robin-Le Guen, F. Bureš, S. Achelle, *J. Org. Chem.* **2017**, *82*, 9435–9451.

[49] R. Claus, J. P. Lewtak, T. J. Muller, J. C. Swarts, *J. Organomet. Chem.* **2013**, *740*, 61–69.

[50] M. Blanchard-Desce, V. Alain, P. V. Bedworth, S. R. Marder, A. Fort, C. Runser, M. Barzoukas, S. Lebus, R. Wortmann, *Chem. Eur. J.* **1997**, *3*, 1091–1104.

[51] A. Isse, A. A. Gennaro, *J. Phys. Chem. B* **2010**, *114*, 7894–7899.

[52] D. T. Sawyer, A. Sobkowiak, J. L. Roberts in *Electrochemistry for Chemists, 2nd edition*, Wiley-Interscience, **1995**.

[53] D. Cvejn, E. Michail, K. Seintis, M. Klikar, O. Pytela, T. Mikysek, N. Almonasy, M. Ludwig, V. Giannetas, M. Fakis, F. Bureš, *RSC Adv.* **2016**, *6*, 12819–12828.

[54] M. J. Frisch, G. W. Trucks, H. B. Schlegel, G. E. Scuseria, M. A. Robb, J. R. Cheeseman, G. Scalmani, V. Barone, G. A. Petersson, H. Nakatsuji, X. Li, M. Caricato, A. V. Marenich, J. Bloino, B. G. Janesko, R. Gomperts, B. Mennucci, H. P. Hratchian, J. V. Ortiz, A. F. Izmaylov, J. L. Sonnenberg, D. Williams-Young, F. Ding, F. Lipparini, F. Egidi, J. Goings, B. Peng, A. Petrone, T. Henderson, D. Ranasinghe, V. G. Zakrzewski, J. Gao, N. Rega, G. Zheng, W. Liang, M. Hada, M. Ehara, K. Toyota, R. Fukuda, J. Hasegawa, M. Ishida, T. Nakajima, Y. Honda, O. Kitao, H. Nakai, T. Vreven, K. Throssell, J. A. Montgomery, Jr., J. E. Peralta, F. Ogliaro, M. J. Bearpark, J. J. Heyd, E. N. Brothers, K. N. Kudin, V. N. Staroverov, T. A. Keith, R. Kobayashi, J. Normand, K. Raghavachari, A. P. Rendell, J. C. Burant, S. S. Iyengar, J. Tomasi, M. Cossi, J. M. Millam, M. Klene, C. Adamo, R. Cammi, J. W. Ochterski, R. L. Martin, K. Morokuma, O. Farkas, J. B. Foresman, D. J. Fox, Gaussian 16, Revision A.03, **2016**.

[55] O. Pytela, OPChem. http://bures.upce.cz/OPgm.

[56] E. Stankovic, S. Toma, R. Van Boxel, I. Asselberghs, A. Persoons, *J. Organomet. Chem.* **2001**, *637–639*, 426–434.

[57] J. Korang, W. R. Grither, R. D. McCulla, *J. Am. Chem. Soc.* **2010**, *132*, 4466–4476.

[58] O. Wennerstrom, V. Boekelheide, R. B. DuVernet, T. Otsubo, J. Lawson, *J. Am. Chem. Soc.* **1978**, *100*, 2457–2464.

Manuscript received: May 21, 2020
Revised manuscript received: July 8, 2020
Accepted manuscript online: July 9, 2020